PAPER

Check for updates

Cu-exchanged RTH-type zeolites for NH₃-selective catalytic reduction of NOₓ: Cu distribution and hydrothermal stability†

Yulong Shan, [ab] Xiaoyan Shi, [ab] Jinpeng Du, [ab] Yunbo Yu [abc] and Hong He*[abc]

The Cu-exchanged RTH-type zeolites (Cu-RTH) were applied in ammonia-selective catalytic reduction (NH₃-SCR) of NOₓ. The effects of Cu loading and distribution on the NOₓ reduction efficiency were investigated. The hydrothermal stabilities of a series of Cu-RTH catalysts were also presented. Excellent NOₓ conversion activity was observed for Cu-RTH catalysts with high Cu loadings (2.5–4.4 wt%) in the temperature range from 150 °C to 550 °C. Two possible sites (α and β species) for Cu^{2+} species were proposed based on the analysis of H₂-TPR and DRIFTS results. The α species next to the 8-membered rings showed significantly higher TOF (turnover frequency) of NO conversion than the β species present next to the rth cage. The Cu-RTH catalysts showed lower activation energies (30–40 kJ mol⁻¹) compared with that of the Cu-SSZ-13 catalyst (~54 kJ mol⁻¹) due to the different zeolite framework structures. After undergoing hydrothermal aging, although the zeolite framework structure stayed stable, the active Cu^{2+} species migrated to inactive sites, which resulted in the loss of NOₓ conversion for the NH₃-SCR reaction. The saturated Cu^{2+}-exchanged Cu₄.₄-RTH catalyst showed the best hydrothermal stability due to the limited Cu^{2+} mobility, which stabilized the active Cu^{2+} species.

1. Introduction

Currently, the removal of NOₓ from diesel engine exhaust, an extremely important environmental issue, faces enormous challenges. Zeolite-based selective catalytic reduction of NOₓ with NH₃ (NH₃-SCR) is an efficient and widely implemented technique for the abatement of NOₓ due to the high NOₓ conversion and hydrothermal stability.[1–7] Since Cu-SSZ-13, a Cu ion-exchanged zeolite with a small-pore chabazite (CHA) framework, was found to have outstanding activity and hydrothermal stability for the reduction of NOₓ in NH₃-SCR, researchers have focused considerably on small-pore metal-exchanged zeolites.[8–15]

During their actual application, the presence of H₂O in the exhaust from diesel particulate filter (DPF) regeneration always damaged the CHA zeolite framework structure by causing the dealumination process. The high hydrothermal stability of small-pore zeolite catalysts is attributed to their specific structures since the constricting dimensions of the special small pores limits the detachment of aluminum hydroxide.[16] Based on this advantage, researchers have focused on many other types of small-pore zeolites, such as KFI,[10] LTA,[9] AEI,[12] RTH,[17] AFX,[18] and ERI,[18] which have also shown NOₓ reduction conversion or hydrothermal stability comparable to Cu-SSZ-13 catalysts in the NH₃-SCR reaction.

Xu *et al.*[19] recently reported an efficient and rapid method of synthesizing small-pore aluminosilicate RTH zeolite, which cansignificantly shorten the crystallization time (50 min at 240 °C), which is beneficial to its practical application as an NH₃-SCR catalyst. Being different from other zeolites (KFI, LTA, AEI, AFX, and ERI) with three-dimensional channels, the RTH-type zeolite has two-dimensional channels with aperture sizes of 0.41 nm × 0.38 nm (8MRs) and 0.56 nm × 0.25 nm (distorted 8MRs), as shown in Scheme 1. The structure of RTH was constructed with a small cage (rth) and a large cage (ite). Therefore, the Cu-exchanged RTH zeolite (Cu-RTH) was expected to have high catalytic properties in the NH₃-SCR reaction due to the 8MR pore channel and its cages. To our knowledge, the studies on Cu-RTH zeolite catalysts used in NH₃-SCR applications have been few. Albarracin-Caballero *et al.*[17] and Jo *et al.*[20] used Cu-RTH zeolites for comparison with SSZ-13 zeolite and other catalysts. However, each literature compared a catalyst with only one Cu-loading value (0.7 wt% and 3.3 wt%, respectively), and limited characterizations

[a] State Key Joint Laboratory of Environment Simulation and Pollution Control, Research Center for Eco-Environmental Sciences, Chinese Academy of Sciences, Beijing, 100085, China. E-mail: honghe@rcees.ac.cn
[b] University of Chinese Academy of Sciences, Beijing 10049, China
[c] Center for Excellence in Regional Atmospheric Environment, Institute of Urban Environment, Chinese Academy of Sciences, Xiamen 361021, China

106 | *Catal. Sci. Technol.*, 2019, 9, 106–115

This journal is © The Royal Society of Chemistry 2019
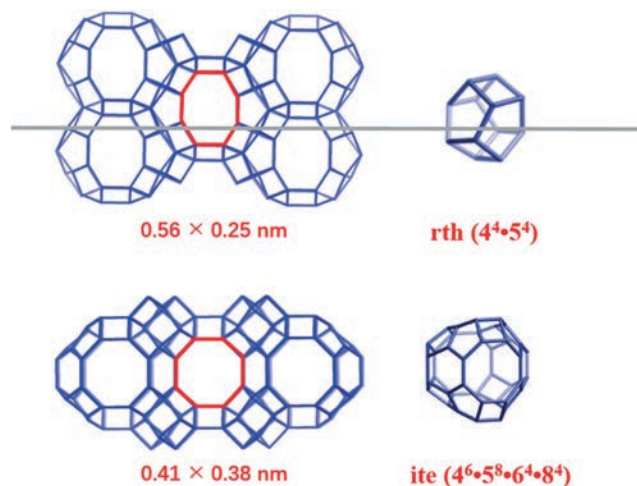
Scheme 1 Two types of 8MR pores and cage structures in the RTH-type zeolite. rth cage consists of 4 four-membered rings and 4 five-membered rings; ite cage consists of 6 four-membered rings, 8 five-membered rings, 4 six-membered rings, and 4 eight-membered rings.

were performed on these catalysts. The zeolite framework structure, Cu^{2+} species distribution, catalytic properties, and hydrothermal stability of Cu-RTH catalysts should be further studied for their dependence on different Cu loadings.

Herein, we systematically investigated Cu-RTH catalysts with different Cu loadings before and after hydrothermal aging. The Cu^{2+} species location and distribution as well as their catalytic properties were studied using H_2-TPR, *in situ* NH_3 absorption DRIFTS measurements, and kinetic studies. Additionally, changes in the Cu^{2+} species and the framework structure after hydrothermal aging were investigated for the Cu-RTH catalysts with different Cu loadings through XRD, ^{27}Al-NMR, and XAFS. We expect to have a better understanding of the structure–activity relationship and optimize the steps for rationally designing Cu-exchanged RTH zeolite catalysts with high activity and hydrothermal stability.

2. Experimental section

2.1. Catalyst preparation

The parent RTH zeolite employed in this study was synthesized following the method reported by Xu *et al.*[19] The obtained Na-RTH zeolite was ion-exchanged with 1 M NH_4NO_3 solution at 80 °C for 8 h to produce NH_4-RTH zeolite. Varying Cu loadings of the Cu-form RTH zeolite were achieved by ion-exchange between NH_4-RTH zeolite and various concentrations of $Cu(CHCOO)_2$ solution (0.05–1.0 M). After the ion-exchange, the catalysts were filtered, washed, and dried in air overnight prior to calcination at 600 °C for 6 h.

For comparison, the Cu-SSZ-13 catalyst was synthesized using a one-pot method.[21] The initial Cu-SSZ-13 catalyst was ion-exchanged with HNO_3 solution (pH = 1). After the ion-exchange, the catalyst was filtered, washed and dried in air overnight prior to calcination at 600 °C for 6 h. The Cu loading and Cu/Al and Si/Al ratios of Cu-RTH catalysts are listed in Table 1.

2.2. Characterization

Powder X-ray diffraction (PXRD) patterns were collected on a computerized Bruker D8 Advance diffractometer with Cu Kα (λ = 0.15406 nm) radiation. The 2θ data from 5° to 40° were collected with a step size of 0.02°. All measurements were performed at ambient temperature. Elemental analyses of the samples (Cu contents, Cu/Al, and Si/Al ratio) were obtained using an inductively coupled plasma instrument (OPTMIA 2000DV) with a radial view of the plasma. The samples were dissolved in strong acid prior to analysis. N_2 adsorption/desorption isotherms of the Cu-RTH samples were measured at 77 K using a Micromeritics ASAP 2020 system. Micropore surface areas and micropore volumes were obtained by the *t*-plot method. Before the measurements, the samples were treated at 300 °C for 5 h. Solid state ^{27}Al and ^{29}Si MAS NMR spectra were collected on a Bruker AVANCE III 400 WB spectrometer equipped with a 4 mm standard bore CP MAS probe head whose X channel was tuned to 156 MHz and 119 MHz for ^{27}Al and ^{29}Si, respectively. The dried and finely powdered samples were packed in the ZrO_2 rotor, closed with a Kel-F cap and spun at 12 kHz. A total of 1000 scans were recorded with 5 s recycle delay for each sample. All ^{27}Al and ^{29}Si MAS NMR chemical shifts were referenced to the resonances of aluminum oxide (Al_2O_3) and TMA standard, respectively.

Temperature-programmed reduction with hydrogen (H_2-TPR) experiments were performed on a Micromeritics AutoChem 2920 chemisorption analyzer. The samples (~50 mg) were loaded into a quartz reactor and exposed to a 10

Table 1 Elemental analysis and micropore areas and volumes of Cu-RTH catalysts

Samples	Cu contents (wt%)	Na contents (wt%)	Cu/Al[a]	Si/Al[a]	Micropore area (m² g⁻¹)[b]	Micropore volume (cm³ g⁻¹)[b]	Micropore area (m² g⁻¹)[c]	Micropore area (m² g⁻¹)[c]
Cu$_{1.0}$-RTH	0.99	0.09	0.10	8.2	519	0.20	—	—
Cu$_{1.4}$-RTH	1.37	0.09	0.15	8.5	528	0.21	—	—
Cu$_{2.5}$-RTH	2.52	0.06	0.27	8.0	547	0.21	510	0.21
Cu$_{3.5}$-RTH	3.46	0.06	0.40	8.2	542	0.21	518	0.21
Cu$_{4.4}$-RTH	4.41	0.05	0.52	8.2	319	0.16	320	0.15

[a] Elements were determined by ICP-AES. [b] For fresh catalysts, calculated by the *t*-plot method. [c] For HTA catalysts, calculated by the *t*-plot method.

This journal is © The Royal Society of Chemistry 2019

Catal. Sci. Technol., 2019, 9, 106–115 | 107

vol% H_2/Ar gas flow at 50 mL min^{-1} after being treated in air at 500 °C for 60 min. Hydrogen consumption was detected by a thermal conductivity detector (TCD), with temperature ramping linearly from ambient temperature to 1000 °C at a rate of 10 °C min^{-1}. The *in situ* diffuse reflectance infrared Fourier transform spectroscopy experiments using molecular NH_3 as the probe (*in situ* NH_3-DRIFTS) were conducted using a Nicolet Is10 instrument equipped with a Smart Collector and an MCT/A detector. Before collecting the spectra, the samples were heated to 500 °C for 1 h in 20% O_2/N_2,and then cooled to 35 °C. Subsequently, the background was collected in pure N_2 and automatically subtracted from the sample spectrum. Then, the sample was exposed to the probe molecule NH_3 until the spectra were unchanged, and then swept out with N_2. All spectra were recorded from 4000 cm^{-1} to 650 cm^{-1} by accumulating 100 scans with a resolution of 4 cm^{-1}.

X-ray absorption fine structure (XAFS) experiments were performed on the BL14W1 beamline of the Shanghai Synchrotron Radiation Facility (SSRF). Using a Si (111) monochromator, the absorption data from −200 eV to 800 eV of the Cu K-edge (8979 eV) was collected at ambient temperature in transmission mode. CuO and Cu_2O were used as reference compounds. X-ray absorption near-edge structure (XANES) data were background-corrected and normalized using the Athena module implemented in the IFFEFIT software package.[22] The extended X-ray absorption fine structure (EXAFS) data and FT of the k^2-weighed data were analyzed and fit using Athena and Artemis (k range of 3–12 Å^{-1}). The amplitude reduction factor (S_0^2) of 0.9 was used for all fitted data sets.

2.3. Catalytic activity test

Standard selective catalytic reduction (SCR) was performed in a fixed-bed quartz flow reactor at atmospheric pressure. A resistance furnace was used to simulate different reaction temperatures. The reactive gas contained 500 ppm NO, 500 ppm NH_3, 5% O_2, 5% H_2O, balance N_2, and the total flow rate was 500 mL min^{-1}. The catalysts were pelletized and sieved to 40–60 mesh size and ~180 mg of catalyst was used, which resulted in a gas hourly space velocity (GHSV) of ~100 000 h^{-1}. An online Nicolet Is10 spectrometer equipped with a heated low volume (0.2 L) multiple-path gas cell (2 m) was used to continuously analyze the effluent gases, including NO, NH_3, NO_2, and N_2O. When the test reaction was in a steady state, FTIR spectra were recorded throughout. NO$_x$ conversion was calculated according to the following equation:

$$NO_x \text{ conversion} = \left(1 - \frac{[NO_x]_{out}}{[NO_x]_{in}}\right) \times 100\% \ (x = 1, 2)$$

Kinetic studies were also conducted on this measurement system. The reaction rates (r), activation energies (E_a), and turnover frequencies (TOF) were calculated based on the following equation:

$$r = -\frac{F}{W}\ln(1-x) \quad k = \frac{r}{[NO]_0} = A_e^{(-E_a/RT)}$$

$$TOF = \frac{F_x}{WM/64}$$

where W is the catalyst weight (g), F is the NO flow rate (mol s^{-1}), x is the NO conversion, $[NO]_0$ is the initial concentration of NO, and M is the weight percent of Cu in the sample. For collecting the hydrothermal stability data, the tested samples were hydrothermally aged (HTA) at 750 °C for 16 h in a 10 vol% H_2O/air feed.

3. Results and discussion

3.1. Standard NH_3-SCR performance and hydrothermal stability

The standard NH_3-SCR activities of Cu-RTH catalysts with varying Cu loading are shown in Fig. 1. It can be seen that $Cu_{1.0}$-RTH and $Cu_{1.4}$-RTH catalysts with low Cu loading exhibited low NO$_x$ conversion at low temperatures (<400 °C) On increasing the Cu loading to 2.5 wt%, a significant increase in NO$_x$ conversion was realized at low temperatures. Further increasing the Cu loading had limited effect on the low temperature activity, but a decrease in NO$_x$ conversion at high temperatures (>450 °C) was observed for these catalysts, probably due to the facile non-selective NH_3 oxidation.[23] Simultaneously, nearly 100% N_2 selectivity was achieved due to the low N_2O production (less than 15 ppm) at all the tested temperatures (150–550 °C) for all the catalysts (Fig. S1†).

Kinetic studies of the NH_3-SCR reaction were performed over the Cu-RTH catalysts with varying Cu loading. Fig. S2† presents the NO$_x$ conversion in a standard NH_3-SCR reaction under rigorous gas hourly space velocity (GHSV) conditions to obtain relatively low NO$_x$ conversion (<20%), which was used to calculate the reaction rates and activation energy (E_a)
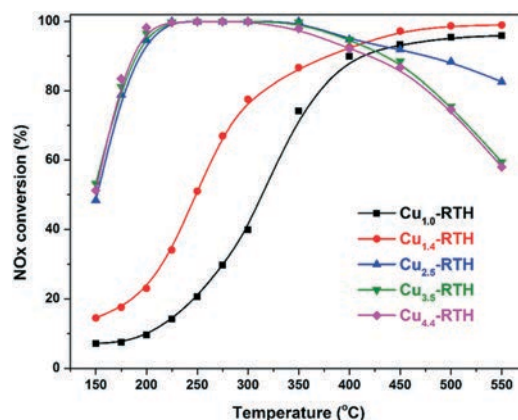

Fig. 1 NO$_x$ conversion of Cu-RTH catalysts with different Cu loadings in the NH_3-SCR reaction. Conditions: 500 ppm of NO, 500 ppm of NH_3, 5% O_2, 5% H_2O, and balanced with N_2. GHSV = 100 000 h^{-1}.

108 | *Catal. Sci. Technol.*, 2019, **9**, 106–115

This journal is © The Royal Society of Chemistry 2019

in the standard SCR reaction. Fig. 2 shows the Arrhenius plots of Cu-RTH with different Cu loadings. It was found that the Cu-RTH catalysts with Cu loadings from 1.0 wt% to 4.4 wt% showed lower activation energies (35–39 kJ mol^{-1}) compared with that of our as-prepared Cu-SSZ-13 catalyst (54 kJ mol^{-1}, Fig. S3†) and other reported Cu-SSZ-13 catalysts.[24] This decrease in activation energy was attributed to the different molecular sieve framework structures of Cu-RTHs, in which the dynamic $[Cu(NH_3)_2]^+$ ions serve as active sites.[25–27]

Generally, the hydrothermal stability of NH_3-SCR catalysts should be improved to meet the requirements for high durability toward moisture at high temperatures for future diesel after-treatment systems.[28,29] In this work, Cu-RTH catalysts with relatively high Cu loadings (2.5 wt%, 3.5 wt%, and 4.4 wt%) were tested after hydrothermal aging because of their high NO_x conversion activities. As shown in Fig. 3, the hydrothermally aged samples showed a sharp decrease in NO_x conversion, indicating severe damage after hydrothermal aging at 750 °C for the Cu-RTH zeolite catalysts. Among the three catalysts, Cu$_{4.4}$-RTH-HTA catalyst exhibited higher NO_x conversion than the other two catalysts. In addition, the NO_x conversion after hydrothermal aging increased with an increase in Cu loading, although fresh catalysts had similar NO_x conversion, particularly at low temperatures. Fig. S4† shows that N_2O formation was still less than 15 ppm for the hydrothermally aged catalysts, indicating excellent N_2 selectivity.

3.2. Characterization of Cu^{2+} species of Cu-RTH catalysts

X-ray absorption spectroscopy (XAS) is an effective technique to determine the local coordination and valence state of Cu species in Cu-based zeolites. Fig. 4 depicts the Cu K-edge XANES spectra and the associated Fourier transforms of EXAFS spectra of the fresh and hydrothermally aged Cu-RTH catalysts measured at ambient temperatures. In addition to ordinary reference samples such as Cu_2O and CuO, Cu-SSZ-13 (Cu: 4.8 wt%, Cu/Al = 0.41) was also used as a reference to compare the Cu coordination and valence states in the two
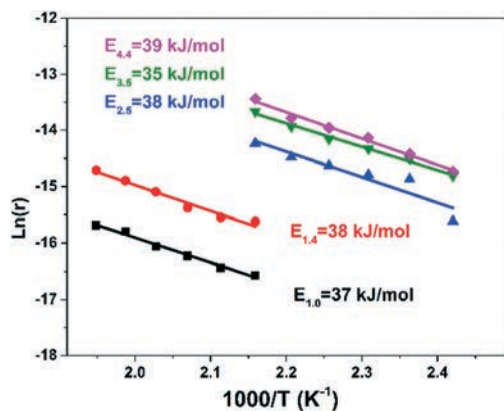

Fig. 3 NO_x conversion of hydrothermally aged Cu–RTH catalysts with different Cu loadings during the NH_3-SCR reaction. Conditions: 500 ppm NO, 500 ppm NH_3, 5% O_2, 5% H_2O, and balanced with N_2. GHSV = 100 000 h^{-1}. Hydrothermal aging conditions: 750 °C, 10% H_2O, and for 16 h.

types of zeolite catalysts, as shown in Fig. S5.† For the fresh samples, a pre-edge feature at 8977.5 eV, which was attributed to the 1s → 3d transition of Cu ions, was characteristic of the presence of Cu(II) (Fig. 4a, magnified profiles).[30] For a series of Cu-RTH catalysts with different Cu loading, this pre-edge feature was unchanged, suggesting that the coordination environment of Cu(II) ions was similar in different samples with varying Cu loadings. Additionally, another weak pre-edge peak was observed at 8983 eV for the Cu-RTH samples, which was assigned to the 2-coordinate isolated Cu(I).[31] It can be seen that the Cu-SSZ-13 catalysts also exhibited a weak peak at 8983 eV (Fig. S4a†). The presence of this feature meant that "self-reduction" of Cu^{2+} species occurred during the process of cooling after calcination. In addition, higher intensities of the pre-feature for Cu-RTH catalysts indicated that more Cu^{2+} ions were converted to Cu^+ than in Cu-SSZ-13 at ambient conditions, suggesting the instability of Cu^{2+} ions in Cu-RTH catalysts. A slight feature at 8986 eV, which was ascribed to the 1s → 4pz electronic transition on 4-coordinate Cu^{2+} (CuO),[31–33] was only observed for the Cu$_{4.4}$-RTH catalyst

Fig. 2 Arrhenius plots of NO_x conversion over Cu-RTH catalysts with different Cu loadings. Normalized reaction rates were calculated using NO_x conversion data (<20%) in high GHSVs, shown in Fig. S2.†
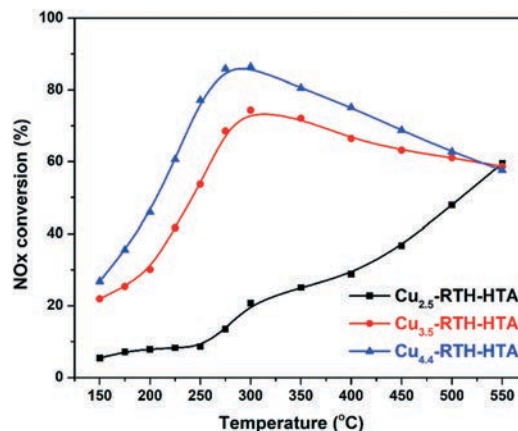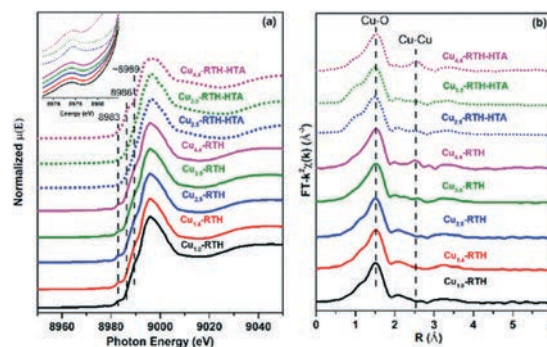

Fig. 4 (a) Cu K-edge XANES spectra and (b) associated Fourier transforms of EXAFS spectra of fresh and hydrothermally aged Cu-RTH catalysts with varying Cu loadings.

This journal is © The Royal Society of Chemistry 2019

Catal. Sci. Technol., 2019, **9**, 106–115 | 109

with highest Cu loading, indicating that high level of Cu^{2+} ion exchange resulted in the formation of a small amount of CuO. The R-space plot of EXAFS data (Fig. 4b) also showed a Cu–Cu bond in the $Cu_{4.4}$-RTH catalyst, while no such Cu–Cu bond was observed for the other fresh catalysts. The broad feature on the absorption edge at 8989 eV was assigned to dehydrated Cu^{2+} species coordinated with the zeolite framework and the hydrated Cu(II)-aqua complex.[13,32,34] The parameters resulting from the experimental data and the simulated fittings of EXAFS spectra are listed in Table S1.† There was almost no difference in the CN (~3.6) and Cu–O bond distance (~1.95 Å) between Cu-RTH and Cu-SSZ-13 catalysts, which indicated that the coordination environments of most Cu species in Cu-RTH are similar to those in Cu-SSZ-13 catalysts.

Among the hydrothermally aged Cu-RTH catalysts, $Cu_{4.4}$-RTH-HTA showed an increase in the feature peak at 8986 eV, indicating CuO_x accumulation during the hydrothermal aging process. However, the feature peak belonging to CuO_x cannot be seen in the XANES spectra for $Cu_{2.5}$ and $Cu_{3.5}$-RTH-HTA catalysts, suggesting no accumulation of CuO_x for $Cu_{2.5}$ and $Cu_{3.5}$-RTH catalysts after hydrothermal aging. The R-space plot of EXAFS data also showed an increased Cu–Cu bond peak intensity in the hydrothermally aged $Cu_{4.4}$-RTH catalyst, while there was no Cu–Cu bond for the other two hydrothermally aged catalysts (Fig. 4b). There was also no significant difference between the fresh and hydrothermally aged Cu-RTH catalysts in terms of the CN (coordination number) and Cu–O distances (Table S1†), indicating that Cu^{2+} in the hydrothermally aged Cu-RTH catalysts was still the dominant form of Cu. Interestingly, the $Cu_{4.4}$-RTH catalyst showed the best hydrothermal stability even though CuO was formed during hydrothermal aging, whereas severe deactivation was observed for the hydrothermally aged $Cu_{2.5}$ and $Cu_{3.5}$-RTH catalysts without CuO_x formation. This phenomenon demonstrated that CuO_x formation was not the main reason for the deactivation of hydrothermally aged $Cu_{2.5}$ and $Cu_{3.5}$-RTH catalysts. Therefore, another reason responsible for the deactivation of these hydrothermal aged Cu-RTH catalysts will be discussed in the next section.

H_2-TPR measurement is an efficient technique to investigate the reducibility and distribution of Cu^{2+} species in Cu-based zeolite catalysts. In H_2-TPR profiles (Fig. 5), the peaks at temperatures lower than 500 °C are attributed to the reduction of Cu^{2+} to Cu^+, and the peaks at temperatures higher than 500 °C are attributed to the reduction of Cu^+ to Cu^0 based on previously published studies.[35–37] As shown in Fig. 5a, the H_2-TPR reduction peak of the fresh Cu-RTH catalysts shows a similar change trend to that of Cu-SSZ-13 with the increase in Cu loading.[36,38] A single reduction peak at around 360 °C was observed for the Cu-RTH catalysts with low Cu loadings (<1.4 wt%), while with increase in Cu loading, another reduction peak appeared at 200 °C. Notably, the intensity of this reduction peak at 200 °C increased when the Cu loading increased from 2.5 wt% to 4.4 wt%, while the intensity of the reduction peak at 360 °C remained almost constant, demonstrating that Cu^{2+} ions preferentially occupied stable ion-exchange sites until saturation; also, another relatively unstable ion-exchange site (peak at 200 °C) was occupied by additional Cu^{2+} ions. The calculation of H_2 consumption is depicted in Fig. S6.† A positive linear relationship between H_2 consumption and Cu loading was observed, which indicated the uniformity of Cu species. It should be noted that a slight amount of CuO was observed in $Cu_{4.4}$-RTH, according to the XAFS results (Fig. 4). The reduction of CuO should exhibit a consumption peak at around 200–300 °C.[3,38,39] It seemed that either there was no distinct CuO reduction peak or the reduction peak might be merged in the peak at 200 °C. Regardless, the amount of CuO for the $Cu_{4.4}$-RTH catalyst was low, as can be seen from the lack of deviation of $Cu_{4.4}$-RTH from the linear relation between H_2 consumption and Cu loading (Fig. S5†) for the Cu-RTH catalysts. Moreover, a wide peak appeared at ~825 °C, attributed to the presence of a variety of Cu^+ species, which would cause the H_2 consumption peak to broaden.
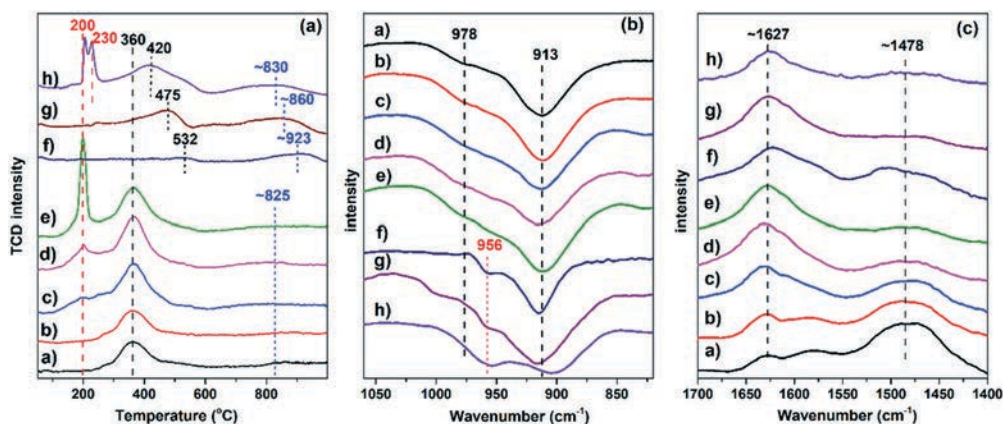

Fig. 5 (a) H_2-TPR profiles, (b) *in situ* DRIFTS spectra of T–O–T vibration regions and (c) acid vibration regions after NH_3 adsorption at 35 °C on fresh and hydrothermally aged Cu-RTH catalysts. a) $Cu_{1.0}$-RTH, b) $Cu_{1.4}$-RTH, c) $Cu_{2.5}$-RTH, d) $Cu_{3.5}$-RTH, e) $Cu_{4.4}$-RTH, f) $Cu_{2.5}$-RTH-HTA, g) $Cu_{3.5}$-RTH-HTA, and h) $Cu_{4.4}$-RTH-HTA.

110 | *Catal. Sci. Technol.*, 2019, **9**, 106–115

This journal is © The Royal Society of Chemistry 2019

After hydrothermal aging at 750 °C, a significant change in the reduction peaks was observed for the Cu-RTH catalysts. The facile reduction peak at 200 °C disappeared for $Cu_{2.5}$-RTH and $Cu_{3.5}$-RTH catalysts after hydrothermal aging. However, the high-temperature H_2 reduction peaks at 532 °C and 475 °C, which were higher than the H_2 reduction peak for fresh samples, were observed for hydrothermally aged $Cu_{2.5}$-RTH and $Cu_{3.5}$-RTH catalysts, respectively. Moreover, for the $Cu_{4.4}$-RTH-HTA catalyst, it was observed that the peak at 200 °C splited into two peaks, which were attributed to the original Cu^{2+} species and CuO_x clusters. This CuO_x formation was identified in the XANES and EXAFS results. Furthermore, the peak at 360 °C of the $Cu_{4.4}$-RTH catalyst also shifted to higher temperature (~420 °C) after hydrothermal aging, similar to the trend observed for $Cu_{2.5}$-RTH and $Cu_{3.5}$-RTH catalysts. The peak for the H_2 reduction of Cu^+ to Cu^0 also shifted to higher temperatures for all Cu-RTH catalysts, indicating that the Cu^{2+} species migrated to more stable sites, where Cu^+ ions were less reducible by H_2. Furthermore, the lower H_2 consumption of hydrothermally aged samples, particularly the $Cu_{2.5}$-RTH-HTA catalyst, indicated that Cu species could not be completely reduced. These unreduced Cu^{2+} species, which were probably the stable Cu–aluminum–oxygen complexes,[3,17] lost their catalytic ability of deNO$_x$.

In situ DRIFTS using NH_3 as the adsorbed probe molecule was also conducted to identify the Cu^{2+} locations. Fig. 5b shows the IR spectra in the zeolite T–O–T bond vibration region after NH_3 was adsorbed onto the Cu-RTH catalysts. Two negative peaks at 978 and 913 cm^{-1} represent the zeolite T–O–T vibration perturbed by Cu^{2+} at different locations because NH_3-solvated Cu^{2+} ions weaken the interaction between Cu^{2+} ions and the zeolite framework.[40,41] From the IR spectra after NH_3 adsorption, it can be seen that the peak intensity at 978 cm^{-1} enhanced, while the peak intensity at 913 cm^{-1} remained stable after saturation of Cu loading of 2.5 wt%. These two resolved peaks in the IR spectra coincide well with the two peaks observed in the H_2-TPR results. Therefore, the DRIFTS experiment using NH_3 as a probe molecule indicated two Cu exchange sites, and the peaks at 978 and 913 cm^{-1} can be possibly attributed to the T–O–T vibration perturbed by the Cu^{2+} species that were reduced at 200 °C and 360 °C, respectively, during the H_2-TPR measurement. For the hydrothermally aged Cu-RTH catalysts, the peak at 978 cm^{-1}, related to Cu^{2+} reduced by H_2 at 200 °C in the H_2-TPR results, disappeared and was accompanied by a new peak appearing at 956 cm^{-1}, which was ascribed to a new stable Cu^{2+} site, probably attributed to the Cu–aluminum–oxygen complexes.[17] After hydrothermal aging, the peak at 913 cm^{-1} changed only slightly, except for the decay observed for $Cu_{4.4}$-RTH due to the formation of CuO_x.

As shown in Fig. 5c, in the N–H bending region, the bands at 1627 cm^{-1} and 1478 cm^{-1} were assigned to molecular NH_3 and NH_4^+ ion adsorbed on the Lewis acid sites and Brønsted acid sites, respectively.[40,42,43] With additional Cu loading, it was observed that the Lewis acid sites, which stem from Cu^{2+} ions, increased accompanied by the decrease in Brønsted

acid sites, indicating that Brønsted acid sites were replaced by Cu^{2+} during the ion exchange process. After hydrothermal aging, the Lewis acid sites of the $Cu_{2.5}$-RTH and $Cu_{3.5}$-RTH catalysts remained almost unchanged, indicating that the Cu^{2+} species still exist even after hydrothermal aging. This result agrees well with the XANES results, where CuO_x was not observed for the hydrothermally aged $Cu_{2.5}$-RTH and $Cu_{3.5}$-RTH catalysts. The decrease in the number of Brønsted acid sites after hydrothermal aging resulted from the dealumination process during hydrothermal aging, which was also observed in the ^{27}Al-NMR measurements (Fig. 7). For the $Cu_{4.4}$-RTH catalyst, the formation of CuO_x identified in XANES (Fig. 4) caused a decrease in the intensity of the peak at 1627 cm^{-1} after hydrothermal aging.

3.3. Characterization of the zeolite structure

The micropore areas and volumes of Cu-RTH zeolite catalysts with different Cu loadings are listed in Table 1. Except for $Cu_{4.4}$-RTH, the samples showed micropore areas of 519–547 $m^2 g^{-1}$, with micropore volumes of 0.20–0.21 $cm^3 g^{-1}$. The lower micropore area and volume of $Cu_{4.4}$-RTH was attributed to pore blocking due to the large amount of copper loading. All Cu-RTH catalysts showed the typical isotherms for microporous materials, as shown in Fig. S7.† After hydrothermal aging, there was no distinct change in the micropore areas or volumes. The typical isotherms of microporous materials were still maintained for hydrothermally aged Cu-RTH catalysts. SEM images (Fig. S8†) of Cu-RTH catalysts also showed no distinct change in morphological features after hydrothermal aging.

XRD patterns of the Cu-RTH samples are exhibited in Fig. 6. Typical diffraction peaks of the RTH zeolite structure were observed for the Cu-RTH catalysts of different Cu loadings with no distinct differences between the samples, indicating the presence of a stable RTH structure after ion exchange. Moreover, the XRD patterns of Cu-RTH catalysts showed no CuO peaks except for that of $Cu_{4.4}$-RTH, with a minor CuO_x peak (magnified XRD profiles in Fig. 6), which indicated well-dispersed Cu species. The formation of CuO for $Cu_{4.4}$-RTH was due to supersaturation during ion exchange
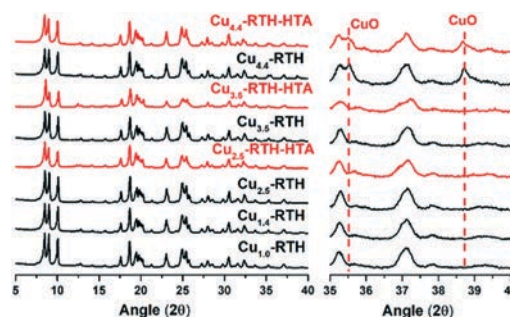

Fig. 6 XRD patterns (left: 2θ = 5–40°) and magnified patterns (right: 2θ = 35–40°) of the Cu-RTH catalysts with different Cu loadings before and after hydrothermal aging.

This journal is © The Royal Society of Chemistry 2019

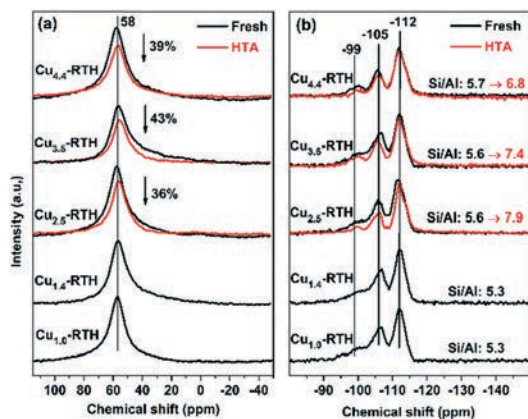*Catal. Sci. Technol.*, 2019, **9**, 106–115 | 111

Fig. 7 (a) ^{27}Al and (b) ^{29}Si-NMR profiles of fresh and hydrothermally aged Cu-RTH catalysts with different Cu loadings.

(Cu/Al = 0.52, 104% ion exchange level), probably resulting in more than one Cu^{2+} ions exchanged to one Al site. The hydrothermally aged Cu-RTH catalysts were also compared. After undergoing hydrothermal aging, although there was a slight decrease in the XRD peak intensity, the XRD patterns of Cu-RTH catalysts showed typical RTH diffraction peaks, indicating that the long-range structural order was maintained. Except for the presence of CuO_x in the $Cu_{4.4}$-RTH-HTA catalyst, there were no typical CuO_x peaks observed for the hydrothermally aged $Cu_{2.5}$-RTH and $Cu_{3.5}$-RTH catalysts.

Next, the local Al and Si coordination was probed by solid state ^{27}Al and ^{29}Si-NMR measurements (Fig. 7). As shown in Fig. 7a, all Cu-RTH catalysts, irrespective of hydrothermally aging, showed only one peak at chemical shift of ~58 ppm, which was attributed to tetrahedral Al (framework Al). After hydrothermal aging, all Cu-RTH catalysts showed a reduced peak at ~58 ppm, while the tetrahedral Al peak still remained for most catalysts, indicating that the integrity of the zeolite structure was maintained. Octahedral Al (at ~0 ppm chemical shift) was not observed after dealumination for the hydrothermally aged Cu-RTH catalysts in the ^{27}Al-NMR profiles, while the peak at ~0 ppm was observed for the hydrothermally aged H-RTH zeolite (Fig. S9†). Therefore, the absence of octahedral Al in Cu-RTH catalysts was probably due to the strong interaction between paramagnetic Cu ions and the as-formed octahedral Al.[3] In addition, the ^{29}Si-NMR spectra are displayed in Fig. 7b. The peaks at −112 ppm, −105 ppm and −99 ppm are ascribed to Si (0Al), Si (1Al), and Si (2Al), respectively.[44] After hydrothermal aging, the peaks at −105 ppm and −99 ppm decreased, which was consistent with the dealumination shown in ^{27}Al-NMR spectra. The framework Si/Al ratio was also calculated based on the deconvoluted ^{29}Si-NMR profiles (Fig. S10†). Cu-RTH catalysts showed an increase in framework Si/Al ratio after hydrothermal aging (5.6 to 7.9, 5.6 to 7.4 and 5.7 to 6.8 for $Cu_{2.5}$-RTH, $Cu_{3.5}$-RTH and $Cu_{4.4}$-RTH catalysts, respectively.), also indicating the dealumination of zeolite structure. Via analysis of the zeolite structure, it was found that although the dealumination process occurred during hydrothermal aging,

the long-range structures and morphological features of Cu-RTH catalysts remained intact, and framework Al was still dominant, indicating a high hydrothermal stability of the zeolite structure.

4. Discussion

4.1. Copper distribution and its relationship with activity

It has been reported that there were two sites for Cu^{2+} location next to a 6-membered ring (6MR) and an 8-membered ring (8MR) in Cu-SSZ-13 catalysts.[36,45] The two Cu^{2+} species could be identified via H_2-TPR and DRIFTS measurements, in which the H_2 consumption peak at ~350 °C and the IR peak at ~900 cm^{-1} are ascribed to the Cu^{2+} species next to 6MR, while the H_2 consumption peak at ~230 °C and the IR peak at 950 cm^{-1} are ascribed to the Cu^{2+} next to 8MR.[36,38,40,41] In the case of Cu-RTH catalysts studied in this work, two different H_2 consumption peaks (200 °C and 360 °C) and two zeolite T–O–T stretching vibrations (978 cm^{-1} and 913 cm^{-1}) perturbed by Cu^{2+} species were also observed. Therefore, analogous to SSZ-13, two sites for Cu^{2+} location in Cu-RTH catalysts are suggested. The H_2 consumption peak at 200 °C and T–O–T vibration at 978 cm^{-1} were attributed to Cu^{2+} next to 8MR (α species), while the H_2 consumption peak at 360 °C and T–O–T vibration at 913 cm^{-1} were attributed to Cu^{2+} next to rth cage (coordinated to 5MR or 6MR, β species). More definitive evidence should be further obtained to clarify the Cu^{2+} location precisely. Nevertheless, the two sites for Cu^{2+} location in Cu-RTH catalysts were confirmed, which we labeled as α and β species.

To investigate the two types of Cu^{2+} species, the TOFs (200–250 °C) of NO conversion in NH_3-SCR reaction were calculated based on the data in Fig. S2† and shown in Fig. 8. The TOFs increased slightly as Cu loading varied from 1.0 wt% to 1.4 wt%. However, when the Cu loading reached 2.5 wt%, there was a significant increase in TOF, which was about quadruple of that of the $Cu_{1.4}$-RTH catalysts. This indicated that another higher active species (α species) appeared rather than an increasing amount of active sites. Therefore,
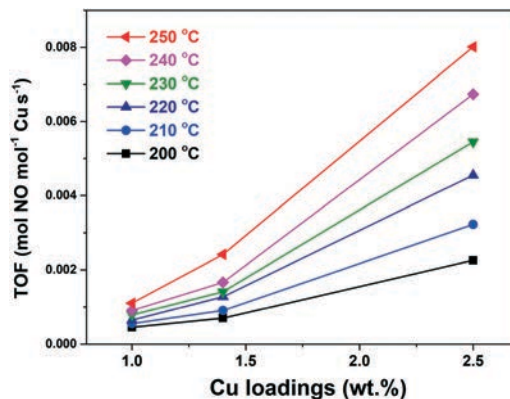

Fig. 8 TOFs of Cu^{2+} of Cu-RTH catalysts as a function of Cu loading. Conditions: 500 ppm NO, 500 ppm NH_3, 5% O_2, 5% H_2O, N_2 balance, and GHSV as shown in Fig. S2.†

112 | *Catal. Sci. Technol.*, 2019, **9**, 106–115

This journal is © The Royal Society of Chemistry 2019

the α species has higher TOF of NO conversion than the β species, resulting in a significant increase in NO_x conversion in the NH_3-SCR reaction for $Cu_{2.5}$-RTH compared with that for $Cu_{1.0}$- and $Cu_{1.4}$-RTH catalysts with low Cu loadings.

4.2. Inactivation mechanism of hydrothermal aging

As shown in Fig. 3, the hydrothermal stability of Cu-RTH catalysts increased with the increase in Cu loading. This result was unexpected because Cu-SSZ-13 catalysts have always showed lower hydrothermal stability with the increase in Cu loading because Cu^{2+} species easily accumulate to form CuO_x, and these CuO_x clusters damaged the zeolite structure.[38,46,47] The effect of Cu loading on hydrothermal aging differs between RTH and CHA zeolites despite the similar nature of the sites of Cu^{2+} species in the two zeolites. Simultaneously, it is worth noting that the $Cu_{4.4}$-RTH catalyst was saturated with Cu ions, with an ion-exchange degree of 104% (Cu/Al = 0.52), and showed the best hydrothermal stability among the tested samples. This phenomenon is consistent with studies on the Cu-LTA catalyst, which showed that fully copper-exchanged samples had the highest hydrothermal stability.[47,48] As shown in the zeolite structure characterization results, it was found that the RTH zeolite structure was hydrothermally stable, though a weak degree of dealumination occurred (Fig. 7). Therefore, the change in active Cu^{2+} species should be primarily responsible for the significant decrease in NO_x conversion after hydrothermal aging. Comparing the H_2-TPR results (Fig. 5) of fresh and hydrothermally aged Cu-RTH catalysts, we found that only the saturated Cu^{2+} ion exchanged RTH zeolite ($Cu_{4.4}$-RTH) maintained its highly active Cu sites (α species) for NO_x conversion, and exhibited a H_2 reduction temperature of 200 °C. Therefore, the $Cu_{4.4}$-RTH catalyst showed the best NH_3-SCR performance after hydrothermal aging (Fig. 3), and the loss of NO_x conversion at high temperatures was attributed to the formation of CuO_x, which caused non-selective NH_3 oxidation. For the $Cu_{2.5}$-RTH and $Cu_{3.5}$-RTH catalysts, however, it was found that the Cu^{2+} species were very stable (high H_2 reduction temperature) after hydrothermal aging. Despite the presence of Cu^{2+}, which was identified in XANES and NH_3-adsorption DRIFTS results, the hydrothermally aged $Cu_{2.5}$-RTH and $Cu_{3.5}$-RTH catalysts lost their NO_x conversion activity due to the presence of more stable and inactive Cu^{2+} species (Cu–aluminum–oxygen complexes). The saturated Cu-exchanged RTH zeolite ($Cu_{4.4}$-RTH) limited the mobility of Cu^{2+} during hydrothermal aging due to the high level of Cu^{2+} ions in the zeolite pores, therefore resulting in some CuO_x accumulation and preservation of highly active Cu^{2+} ions (α species). For the $Cu_{2.5}$-RTH and $Cu_{3.5}$-RTH catalysts, in contrast, the Cu^{2+} species easily migrated to more stable sites, in which Cu^{2+} showed low activity for NO_x reduction after hydrothermal aging. Based on these observations, it may be a good strategy to use other substituting metal ions to partially occupy the exchanged sites and limit Cu mobility in order to increase the hydrothermal stability, which should be explored in future.

5. Conclusions

In this work, Cu-RTH catalysts with varied Cu loadings showed low activation energies (30–40 kJ mol^{-1}) in the NH_3-SCR reaction for NO_x elimination. Two possible sites for Cu^{2+} in the Cu-RTH catalysts were suggested to be located next to 8MR (α species) and rth cage (β species). The α species has a significantly higher TOF of NO conversion than the β species. After hydrothermal aging, the zeolite framework structure changed only slightly, but a significant decrease in NO_x conversion was observed, which was attributed to the change in Cu^{2+} species. The Cu^{2+} species, particularly the α species, were easily movable and transferred to more stable sites during hydrothermal aging, therefore resulting in inactive Cu^{2+} species for NO_x reduction. The fully Cu-exchanged $Cu_{4.4}$-RTH catalyst (saturation, Cu/Al = 0.52) showed the best hydrothermal stability, which was attributed to the preservation of highly active Cu^{2+} species (α species) due to the limited Cu^{2+} ions mobility during hydrothermal aging.

Conflicts of interest

There are no conflicts to declare.

Acknowledgements

Notes and references

1 J. Park, H. Park, J. Baik, I. Nam, C. Shin, J. Lee, B. Cho and S. Oh, Hydrothermal stability of CuZSM5 catalyst in reducing NO by NH_3 for the urea selective catalytic reduction process, *J. Catal.*, 2006, **240**, 47–57.

2 J. H. Kwak, R. G. Tonkyn, D. H. Kim, J. Szanyi and C. H. F. Peden, Excellent activity and selectivity of Cu-SSZ-13 in the selective catalytic reduction of NOx with NH_3, *J. Catal.*, 2010, **275**, 187–190.

3 J. H. Kwak, D. Tran, S. D. Burton, J. Szanyi, J. H. Lee and C. H. F. Peden, Effects of hydrothermal aging on NH_3-SCR reaction over Cu/zeolites, *J. Catal.*, 2012, **287**, 203–209.

4 X. Shi, F. Liu, L. Xie, W. Shan and H. He, NH_3-SCR performance of fresh and hydrothermally aged Fe-ZSM-5 in standard and fast selective catalytic reduction reactions, *Environ. Sci. Technol.*, 2013, **47**, 3293–3298.

5 L. Xie, F. Liu, L. Ren, X. Shi, F. S. Xiao and H. He, Excellent performance of one-pot synthesized Cu-SSZ-13 catalyst for the selective catalytic reduction of NOx with NH_3, *Environ. Sci. Technol.*, 2014, **48**, 566–572.

6 C. Yin, P. Cheng, X. Li and R. T. Yang, Selective catalytic reduction of nitric oxide with ammonia over high-activity Fe/SSZ-13 and Fe/one-pot-synthesized Cu-SSZ-13 catalysts, *Catal. Sci. Technol.*, 2016, **6**, 7561–7568.

7 S. Han, Q. Ye, S. Cheng, T. Kang and H. Dai, Effect of the hydrothermal aging temperature and Cu/Al ratio on the

This journal is © The Royal Society of Chemistry 2019

Catal. Sci. Technol., 2019, **9**, 106–115 | 113

hydrothermal stability of CuSSZ-13 catalysts for NH$_3$-SCR, *Catal. Sci. Technol.*, 2017, **7**, 703–717.

8 F. Gao, Y. Zheng, R. K. Kukkadapu, Y. Wang, E. D. Walter, B. Schwenzer, J. Szanyi and C. H. F. Peden, Iron Loading Effects in Fe/SSZ-13 NH$_3$-SCR Catalysts: Nature of the Fe Ions and Structure–Function Relationships, *ACS Catal.*, 2016, **6**, 2939–2954.

9 D. Jo, T. Ryu, G. T. Park, P. S. Kim, C. H. Kim, I.-S. Nam and S. B. Hong, Synthesis of High-Silica LTA and UFI Zeolites and NH$_3$–SCR Performance of Their Copper-Exchanged Form, *ACS Catal.*, 2016, **6**, 2443–2447.

10 J. Kim, S. J. Cho and D. H. Kim, Facile Synthesis of KFI-type Zeolite and Its Application to Selective Catalytic Reduction of NOx with NH$_3$, *ACS Catal.*, 2017, **7**, 6070–6081.

11 J. H. Lee, Y. J. Kim, T. Ryu, P. S. Kim, C. H. Kim and S. B. Hong, Synthesis of zeolite UZM-35 and catalytic properties of copper-exchanged UZM-35 for ammonia selective catalytic reduction, *Appl. Catal., A*, 2017, **200**, 428–438.

12 M. Moliner, C. Franch, E. Palomares, M. Grill and A. Corma, Cu-SSZ-39, an active and hydrothermally stable catalyst for the selective catalytic reduction of NOx, *Chem. Commun.*, 2012, **48**, 8264–8266.

13 R. Q. Zhang, J. Szanyi, F. Gao and J. S. McEwen, The interaction of reactants, intermediates and products with Cu ions in Cu-SSZ-13 NH3 SCR catalysts: an energetic and ab initio X-ray absorption modeling study, *Catal. Sci. Technol.*, 2016, **6**, 5812–5829.

14 A. Shishkin, H. Kannisto, P.-A. Carlsson, H. Harelind and M. Skoglundh, Synthesis and functionalization of SSZ-13 as an NH$_3$-SCR catalyst, *Catal. Sci. Technol.*, 2014, **4**, 3917–3926.

15 R. Oord, I. C. ten Have, J. M. Arends, F. C. Hendriks, J. Schmidt, I. Lezcano-Gonzalez and B. M. Weckhuysen, Enhanced activity of desilicated Cu-SSZ-13 for the selective catalytic reduction of NOx and its comparison with steamed Cu-SSZ-13, *Catal. Sci. Technol.*, 2017, **7**, 3851–3862.

16 D. W. Fickel, E. D'Addio, J. A. Lauterbach and R. F. Lobo, The ammonia selective catalytic reduction activity of copper-exchanged small-pore zeolites, *Appl. Catal., A*, 2011, **102**, 441–448.

17 J. D. Albarracin-Caballero, I. Khurana, J. R. Di Iorio, A. J. Shih, J. E. Schmidt, M. Dusselier, M. E. Davis, A. Yezerets, J. T. Miller, F. H. Ribeiro and R. Gounder, Structural and kinetic changes to small-pore Cu-zeolites after hydrothermal aging treatments and selective catalytic reduction of NOx with ammonia, *React. Chem. Eng.*, 2017, **2**, 168–179.

18 N. Martín, C. Paris, P. N. R. Vennestrøm, J. R. Thøgersen, M. Moliner and A. Corma, Cage-based small-pore catalysts for NH3 -SCR prepared by combining bulky organic structure directing agents with modified zeolites as reagents, *Appl. Catal., A*, 2017, **217**, 125–136.

19 F. Xiao, H. Xu, Q. Wu, Y. Chu, J.-g. Jiang, L. Zhang, S. Pan, C. Zhang, L. Zhu, F. Deng, X. Meng, S. Maurer, R. McGuire, A.-N. Parvulescu and U. Mueller, Efficient synthesis of aluminosilicate RTH zeolite with good catalytic performances in NH$_3$-SCR and MTO reactions, *J. Mater. Chem. A*, 2018, **6**, 8705–8711.

20 D. Jo, J. B. Lim, T. Ryu, I.-S. Nam, M. A. Camblor and S. B. Hong, Unseeded hydroxide-mediated synthesis and CO$_2$ adsorption properties of an aluminosilicate zeolite with the RTH topology, *J. Mater. Chem. A*, 2015, **3**, 19322–19329.

21 L. Ren, L. Zhu, C. Yang, Y. Chen, Q. Sun, H. Zhang, C. Li, F. Nawaz, X. Meng and F. S. Xiao, Designed copper-amine complex as an efficient template for one-pot synthesis of Cu-SSZ-13 zeolite with excellent activity for selective catalytic reduction of NOx by NH$_3$, *Chem. Commun.*, 2011, **47**, 9789–9791.

22 M. Newville, Interactive XAFS Analysis and FEFF Fitting, *J. Synchrotron Radiat.*, 2001, 322–324.

23 J. H. Kwak, D. Tran, J. Szanyi, C. H. F. Peden and J. H. Lee, The Effect of Copper Loading on the Selective Catalytic Reduction of Nitric Oxide by Ammonia Over Cu-SSZ-13, *Catal. Lett.*, 2012, **142**, 295–301.

24 F. Gao, E. D. Walter, M. Kollar, Y. Wang, J. Szanyi and C. H. F. Peden, Understanding ammonia selective catalytic reduction kinetics over Cu/SSZ-13 from motion of the Cu ions, *J. Catal.*, 2014, **319**, 1–14.

25 C. Paolucci, I. Khurana, A. A. Parekh, S. Li, A. J. Shih, H. Li, J. R. D. Iorio, J. D. Albarracin-Caballero, A. Yezerets, J. T. Miller, W. N. Delgass, F. H. Ribeiro, W. F. Schneider and R. Gounder, Dynamic multinuclear sites formed by mobilized copper ions in NOx selective catalytic reduction, *Science*, 2017, **357**, 898–903.

26 F. Gao, D. Mei, Y. Wang, J. Szanyi and C. H. Peden, Selective Catalytic Reduction over Cu/SSZ-13: Linking Homo- and Heterogeneous Catalysis, *J. Am. Chem. Soc.*, 2017, **139**, 4935–4942.

27 C. Paolucci, A. A. Parekh, I. Khurana, J. R. Di Iorio, H. Li, J. D. Albarracin Caballero, A. J. Shih, T. Anggara, W. N. Delgass, J. T. Miller, F. H. Ribeiro, R. Gounder and W. F. Schneider, Catalysis in a Cage: Condition-Dependent Speciation and Dynamics of Exchanged Cu Cations in SSZ-13 Zeolites, *J. Am. Chem. Soc.*, 2016, **138**, 6028–6048.

28 A. M. Beale, F. Gao, I. Lezcano-Gonzalez, C. H. Peden and J. Szanyi, Recent advances in automotive catalysis for NO$_x$ emission control by small-pore microporous materials, *Chem. Soc. Rev.*, 2015, **44**, 7371–7405.

29 J. Wang, H. Zhao, G. Haller and Y. Li, Recent advances in the selective catalytic reduction of NO$_x$ with NH$_3$ on Cu-Chabazite catalysts, *Appl. Catal., A*, 2017, **202**, 346–354.

30 E. Borfecchia, K. A. Lomachenko, F. Giordanino, H. Falsig, P. Beato, A. V. Soldatov, S. Bordiga and C. Lamberti, Revisiting the nature of Cu sites in the activated Cu-SSZ-13 catalyst for SCR reaction, *Chem. Sci.*, 2015, **6**, 548–563.

31 S. A. Bates, A. A. Verma, C. Paolucci, A. A. Parekh, T. Anggara, A. Yezerets, W. F. Schneider, J. T. Miller, W. N. Delgass and F. H. Ribeiro, Identification of the active Cu site in standard selective catalytic reduction with ammonia on Cu-SSZ-13, *J. Catal.*, 2014, **312**, 87–97.

32 I. Lezcano-Gonzalez, U. Deka, H. E. van der Bij, P. Paalanen, B. Arstad, B. M. Weckhuysen and A. M. Beale, Chemical deactivation of Cu-SSZ-13 ammonia selective catalytic reduction (NH$_3$-SCR) systems, *Appl. Catal., A*, 2014, **154–155**, 339–349.

33 I. Lezcano-Gonzalez, D. S. Wragg, W. A. Slawinski, K. Hemelsoet, A. Van Yperen-De Deyne, M. Waroquier, V. Van Speybroeck and A. M. Beale, Determination of the Nature of the Cu Coordination Complexes Formed in the Presence of NO and NH$_3$ within SSZ-13, *J. Phys. Chem. C*, 2015, **119**, 24393–24403.

34 J. H. Kwak, T. Varga, C. H. F. Peden, F. Gao, J. C. Hanson and J. Szanyi, Following the movement of Cu ions in a SSZ-13 zeolite during dehydration, reduction and adsorption: A combined in situ TP-XRD, XANES/DRIFTS study, *J. Catal.*, 2014, **314**, 83–93.

35 L. Xie, F. Liu, X. Shi, F.-S. Xiao and H. He, Effects of post-treatment method and Na co-cation on the hydrothermal stability of Cu–SSZ-13 catalyst for the selective catalytic reduction of NOx with NH$_3$, *Appl. Catal., A*, 2015, **179**, 206–212.

36 J. Hun Kwak, H. Zhu, J. H. Lee, C. H. Peden and J. Szanyi, Two different cationic positions in Cu-SSZ-13?, *Chem. Commun.*, 2012, **48**, 4758–4760.

37 F. Gao, E. D. Walter, E. M. Karp, J. Luo, R. G. Tonkyn, J. H. Kwak, J. Szanyi and C. H. F. Peden, Structure–activity relationships in NH$_3$-SCR over Cu-SSZ-13 as probed by reaction kinetics and EPR studies, *J. Catal.*, 2013, **300**, 20–29.

38 Y. J. Kim, J. K. Lee, K. M. Min, S. B. Hong, I.-S. Nam and B. K. Cho, Hydrothermal stability of CuSSZ13 for reducing NOx by NH$_3$, *J. Catal.*, 2014, **311**, 447–457.

39 T. Zhang, F. Qiu and J. Li, Design and synthesis of core-shell structured meso-Cu-SSZ-13@mesoporous aluminosilicate catalyst for SCR of NO$_x$ with NH$_3$: Enhancement of activity, hydrothermal stability and propene poisoning resistance, *Appl. Catal., A*, 2016, **195**, 48–58.

40 J. Luo, D. Wang, A. Kumar, J. Li, K. Kamasamudram, N. Currier and A. Yezerets, Identification of two types of Cu sites in Cu/SSZ-13 and their unique responses to hydrothermal aging and sulfur poisoning, *Catal. Today*, 2016, **267**, 3–9.

41 J. Luo, F. Gao, K. Kamasamudram, N. Currier, C. H. F. Peden and A. Yezerets, New insights into Cu/SSZ-13 SCR catalyst acidity. Part I: Nature of acidic sites probed by NH$_3$ titration, *J. Catal.*, 2017, **348**, 291–299.

42 D. Wang, L. Zhang, K. Kamasamudram and W. S. Epling, In Situ-DRIFTS Study of Selective Catalytic Reduction of NO$_x$ by NH$_3$ over Cu-Exchanged SAPO-34, *ACS Catal.*, 2013, **3**, 871–881.

43 L. Zhang, D. Wang, Y. Liu, K. Kamasamudram, J. Li and W. Epling, SO$_2$ poisoning impact on the NH$_3$-SCR reaction over a commercial Cu-SAPO-34 SCR catalyst, *Appl. Catal., A*, 2014, **156-157**, 371–377.

44 J. Klinowski, Solid-State NMR studies of molecular sieve catalysts, *Chem. Rev.*, 1991, **91**, 1459–1479.

45 C. W. Andersen, M. Bremholm, P. N. Vennestrom, A. B. Blichfeld, L. F. Lundegaard and B. B. Iversen, Location of Cu(2+) in CHA zeolite investigated by X-ray diffraction using the Rietveld/maximum entropy method, *IUCrJ*, 2014, **1**, 382–386.

46 J. Song, Y. Wang, E. D. Walter, N. M. Washton, D. Mei, L. Kovarik, M. H. Engelhard, S. Prodinger, Y. Wang, C. H. F. Peden and F. Gao, Toward Rational Design of Cu/SSZ-13 Selective Catalytic Reduction Catalysts: Implications from Atomic-Level Understanding of Hydrothermal Stability, *ACS Catal.*, 2017, **7**, 8214–8227.

47 T. Ryu, N. H. Ahn, S. Seo, J. Cho, H. Kim, D. Jo, G. T. Park, P. S. Kim, C. H. Kim, E. L. Bruce, P. A. Wright, I. S. Nam and S. B. Hong, Fully Copper-Exchanged High-Silica LTA Zeolites as Unrivaled Hydrothermally Stable NH3-SCR Catalysts, *Angew. Chem., Int. Ed.*, 2017, **56**, 3256–3260.

48 N. H. Ahn, T. Ryu, Y. Kang, H. Kim, J. Shin, I.-S. Nam and S. B. Hong, The Origin of an Unexpected Increase in NH$_3$–SCR Activity of Aged Cu-LTA Catalysts, *ACS Catal.*, 2017, **7**, 6781–6785.

This journal is © The Royal Society of Chemistry 2019

Catal. Sci. Technol., 2019, **9**, 106–115 | 115